

Spin-flip Effects in the Mesoscopic Spin-Interferometer.

A.Aldea^{*,†}, M.Tolea^{*} and J.Zittartz[†]

^{*} National Institute of Materials Physics, POBox MG7, Bucharest-Magurele, Romania

[†] Institut für Theoretische Physik, Universität zu Köln, D-50923 Köln, Germany

We investigate the properties of the electron spin-transmission through an Aharonov-Bohm interferometer with an embedded two-dimensional multilevel quantum dot containing magnetic impurities. A suitable formalism is developed. The amplitude and the phase of the flip- and nonflip-transmittance are calculated numerically as function of the magnetic field and the gate potential applied on the dot. The effects induced by the exchange interaction to spin-dependent magnetoconductance fluctuations and transmittance phase are shown.

PACS numbers: 85.75.-d, 73.23.-b

I. INTRODUCTION

The spin interferometry in mesoscopic systems is expected to give new insights in the field of nano-physics. We approach this problem in a ring-dot geometry with the aim to identify new properties of the Aharonov-Bohm oscillations due to the presence of magnetic impurities within a multiple level dot; we show also the ensemble of parameters that determine the problem.

The Aharonov-Bohm interferometer with embedded quantum dot has been used to study the phase of the electron transmission as a voltage applied on the dot is varied [1, 2], however no attention was paid till now to the spin transmittance or even to magnetoconductance fluctuations in such tunable systems, where the finite size of the dot plays an effective role. The set-up is sketched in Fig.1; the dot contains magnetic impurities, which implies an exchange interaction between the spin of the free incident electron and the localized spins in the dot. In the real systems, the dot has a finite size so that the electron crosses the dot along different paths, with implications for the resulting interference pattern. This is why the usual model which assimilates the dot with a one-site impurity (with at most two-orbitals) [3] cannot capture all the interference effects in actual ring-dot systems. The price to be paid for considering a realistic geometry for the dot is to make a single electron approach; we mention in this respect the recent paper by Nakanishi et al [4] who uses a continuous model for the study of the Fano effects.

The spin-dependent transmittance amplitude can be written as a superposition of all possible paths:

$$t_{\sigma,\sigma'} = t^1 \delta_{\sigma,\sigma'} + \sum_{k \in 2} t_{\sigma,\sigma'}^k e^{i(\Phi + \Delta\phi_{\sigma,\sigma'}^k)}, \quad (1)$$

where t^1 is the amplitude of the transmittance through the lower arm which conserves the spin, Φ is the magnetic flux that pierces the ring and $\Delta\phi$ is the supplementary contribution of the dot, where spin-flip processes may occur.

The aspect of the output depends on the magnetic field

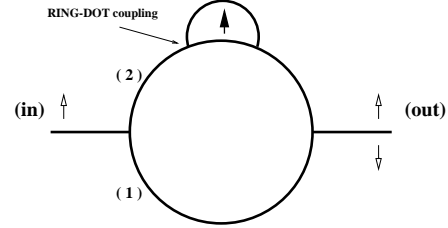


FIG. 1: The sketch of the spin interferometer; the incident electron is spin-polarized; the dot contains a localized magnetic impurity which couples with the spin of the free electron. A magnetic field pierces perpendicularly the ring and the dot.

that pierces both the ring and the dot and on the gate potential applied on the dot; at the same time, it is strongly controlled by the strength of the ring-dot coupling (τ) and the energy of the incident electron (E_F).

As explained throughout the paper, the range of parameters is large and different regimes can be studied. For instance, in the case of small τ , one may consider that the ring-dot coupling only produces broadening and slight shifts in the spectrum of the individual dot. In the opposite case, this picture is no longer valid and the ring-dot system has to be regarded as a unique coherent system, meaning that τ must be considered in all powers of the perturbation series. The hybridization depends on the electric potential V_g since the applied potential shifts the dot levels. However, for a two-dimensional quantum dot, the same can be achieved by the variation of the magnetic flux, as put into evidence by a recent experiment carried out in the same ring-dot geometry [5]. We shall focus our study on the spin dependent magnetoconductance as function of flux at fixed gate potential.

Since several energy scales come into the problem, one has to establish from the very beginning the assumptions of the approach. We consider that the main processes which are to be taken into account are the orbital motion in magnetic field along the ring and inside the dot, and the exchange interaction J . We assume that the Zeeman effect is less effective than the exchange, i.e.

$g\mu_B B/J < 1$ [6]; the spin-orbit interaction is neglected, too. We use a tight-binding (TB) description that proved to be efficient in describing interference effects for differently shaped systems and in the presence of disorder and interactions [7, 8]. The magnetic field (in the Landau gauge) appears as a Peierls phase Φ_{ij} in the hopping integral, and only the next-neighbor hopping is considered. The dot is an island of 3×5 sites attached on the external side of the ring, with the magnetic impurity placed in the middle. The dot area represents 15% from the area of the whole device. The Hamiltonian of the ring-dot system in perpendicular magnetic field reads:

$$H = \sum_{\langle i,j \rangle, \sigma} w_{ij, \sigma} e^{i2\pi\Phi_{ij}} c_{i, \sigma}^\dagger c_{j, \sigma} + \sum_{\sigma, i \in QD} V_g c_{i, \sigma}^\dagger c_{i, \sigma} - J (c_{n\uparrow}^\dagger c_{n\uparrow} - c_{n\downarrow}^\dagger c_{n\downarrow}) S_n^z - J (c_{n\downarrow}^\dagger c_{n\uparrow} S_n^+ + H.c.),$$

$$n \in QD. \quad (2)$$

where c_i^\dagger (c_i) are creation (annihilation) operators in localized states indexed by i ; the index n is devoted to the site of the dot where the magnetic impurity -called also the 'flipper'- is placed. The first term describes both the 1D ring and the dot ($i, j = 1..N$), the second term allows for the gate potential on the dot and the last terms represent the local spin-spin interaction. The hopping integral will be taken as energy unit, i.e. $w_{ij, \sigma} = 1$ for any pair (i,j) excepting at the contacts between the dot and the ring, where $w = \tau \in [0, 1]$.

The outline of this paper is as follows. In section II we adapt the formalism used previously for the spinless problem [9] to the spin transport through meso systems. This yields a fast way to obtain numerical results in the presence of spin scattering based on the calculation of the resolvent in a reduced Hilbert space and Landauer-Büttiker formalism. The existence of different regimes is shown. Section III introduces the singlet and triplet operators and expresses the flip and non-flip processes in terms of two-time Green (singlet & triplet) functions with their corresponding equations of motion. We also show how the single electron scattering problem is recovered from the general many-body scheme. An application is done for an analytically soluble model in sec IV, with the aim to produce hints for the ring+2Ddot interferometer. This complex system is studied numerically in sec V, where spectral and transport properties are shown, indicating the role of different parameters like the Fermi energy and the coupling constant τ . The main conclusions are presented in the last section.

II. SPIN TUNNELING IN THE RESOLVENT REPRESENTATION AND DISCUSSION OF DIFFERENT REGIMES

In what follows we shall reduce the many-body problem to the physical situation when a "test" electron car-

rying the spin σ passes through the interferometer and interacts via the exchange J with the localized spin S . So we have to project the Hamiltonian on the product Hilbert space describing a single free spin and a single localized spin: $\mathcal{H}_{2N}^\sigma \otimes \mathcal{H}_{2S+1}^S$. This space is spanned by the basis $\{|i, \sigma\rangle\} \otimes \{|\chi_S\rangle\}$. For this reason, in the present section we shall use the bra/ket representation instead of the creation/annihilation operators.

For the calculation of the transmittance (in the Landauer-Büttiker formalism) additional terms are needed in order to describe the external leads and their contacts to the ring-dot system. It is however sufficient to use an effective Hamiltonian depending only on the degrees of freedom of the ring-dot, but containing the whole information about the leads and lead-ring coupling in a non-Hermitian term [9]:

$$H^{eff} = H + \tau_0^2 \sum_{\alpha, \sigma} e^{-iq} |\alpha\sigma\rangle\langle\alpha\sigma|, \quad (3)$$

where q is defined by $E_F = 2\cos(q)$ and $\{\alpha\}$ denotes the sites where the leads are connected to the system. τ_0 is the parameter describing the lead-ring coupling and it will be taken $\tau_0 = 1$. Taking into account that the lead-ring coupling conserves the spin, only the diagonal elements are modified by the coupling τ_0 , and one can define the non-flip effective Hamiltonian :

$$H_{\uparrow\uparrow}^{eff} = \sum_{\langle i,j \rangle} w_{ij, \uparrow} e^{i2\pi\Phi_{ij}} |i \uparrow\rangle\langle j \uparrow| + \sum_{i \in QD} V_g |i \uparrow\rangle\langle i \uparrow| - JS_n^z |n \uparrow\rangle\langle n \uparrow| + \tau_0^2 \sum_{\alpha} e^{-iq} |\alpha \uparrow\rangle\langle \alpha \uparrow|, \quad (4)$$

while the spin-flip Hamiltonian is simply:

$$H_{\uparrow\downarrow}^{eff} = H_{\downarrow\uparrow} = -JS_n^- |n \uparrow\rangle\langle n \downarrow|. \quad (5)$$

In order to calculate the spin transmittance through the complex system one needs to know the retarded resolvent Green function:

$$G^+(E) = (E - H^{eff} + i0)^{-1}.$$

Then, in order to express the different flip and non-flip tunneling processes we define the 2x2 matrix Green function

$$G_{\sigma, \sigma'}(z) =: \langle \sigma | G(z) | \sigma' \rangle$$

for which Dyson equations can be written immediately and the expressions for the nonflip $G_{\uparrow\uparrow}(z)$ and flip $G_{\uparrow\downarrow}(z)$ read :

$$G_{\uparrow\uparrow}(z) = \left(z - H_{\uparrow\uparrow}^{eff} - H_{\uparrow\downarrow}(z - H_{\downarrow\downarrow}^{eff})^{-1} H_{\downarrow\uparrow} \right)^{-1}$$

$$G_{\uparrow\downarrow}(z) = G_{\uparrow\uparrow}(z) H_{\uparrow\downarrow}^{eff} (z - H_{\downarrow\downarrow}^{eff})^{-1}. \quad (6)$$

Using (5) these equations can be further expressed as:

$$\begin{aligned}
G_{\uparrow\uparrow}(z) &= \left(z - H_{\uparrow\uparrow}^{eff} - J^2 S_n^- |n \uparrow\rangle \langle n \downarrow| \frac{1}{z - H_{\downarrow\downarrow}^{eff}} |n \downarrow\rangle \langle n \uparrow| S_n^+ \right)^{-1}, \\
G_{\uparrow\downarrow}(z) &= -J G_{\uparrow\uparrow}(z) S_n^- |n \uparrow\rangle \langle n \downarrow| \frac{1}{z - H_{\downarrow\downarrow}^{eff}}. \quad (7)
\end{aligned}$$

In order to proceed we shall consider $S_n = 1/2$. Since the exchange interaction conserves the total spin and its projection on the z-axis, there are three different tunneling processes between the following *in* and *out* states:

$$\begin{aligned}
a) & |\alpha \uparrow\uparrow\rangle \rightarrow |\alpha' \uparrow\uparrow\rangle \quad (\text{non-flip process}) \\
b) & |\alpha \uparrow\downarrow\rangle \rightarrow |\alpha' \uparrow\downarrow\rangle \quad (\text{non-flip process}) \\
c) & |\alpha \uparrow\downarrow\rangle \rightarrow |\alpha' \downarrow\uparrow\rangle \quad (\text{flip process})
\end{aligned} \quad (8)$$

The first two processes contribute to the non-flip transmittance while the third process to the flip transmittance. We remind that the pair of sites (α, α') represent the points where the ring is connected to the terminals and that the incoming spin is supposed to be polarized in the $up(\uparrow)$ -state. The notation $|\uparrow\rangle, |\downarrow\rangle$ stands for the eigenvectors of the impurity spin operator S_n^z .

Finally, the spin transmittance is obtained by calculating the matrix elements of $G_{\sigma,\sigma'}$ in (7) between these *in* and *out* states, and using them in the general expression of the Landauer-Büttiker formula:

$$T_{\sigma,\sigma',S,S'}(E, \Phi) = 4\tau_0^4 \sin^2 q |\langle \alpha, S | G_{\sigma\sigma'}^+(E) | \alpha', S' \rangle|^2 \quad (9)$$

As an explicit example of how the matrix elements look like, we give :

$$\begin{aligned}
& \langle \alpha \uparrow\uparrow | G_{\sigma\sigma}(z) | \alpha' \uparrow\uparrow \rangle = \\
& \langle \alpha \uparrow | \left(z - \sum_{\langle i,j \rangle} w_{ij,\uparrow} e^{i2\pi\Phi_{ij}} |i \uparrow\rangle \langle j \uparrow| - \right. \\
& \left. \tau_0^2 e^{ik} \sum_{\alpha_1} |\alpha_1 \uparrow\rangle \langle \alpha_1 \uparrow| + \frac{J}{2} |n \uparrow\rangle \langle n \uparrow| \right)^{-1} | \alpha' \uparrow \rangle. \quad (10)
\end{aligned}$$

The value of this Green function element can be calculated by the direct numerical inversion of the matrix which is now completely known.

The Aharonov-Bohm interference is impossible when the dot does not transmit, since the circulation of the vector potential is to be considered along a closed contour. The transmittance of the dot can be controlled by changing the gate potential applied on the dot. Therefore, the transmittance spectrum in the plane of the variables V_g (gate potential) and Φ (magnetic flux through the ring) has to be analyzed first.

The space of parameters is covered by τ (ring-dot coupling), J (exchange) and E_F (the Fermi level imposed

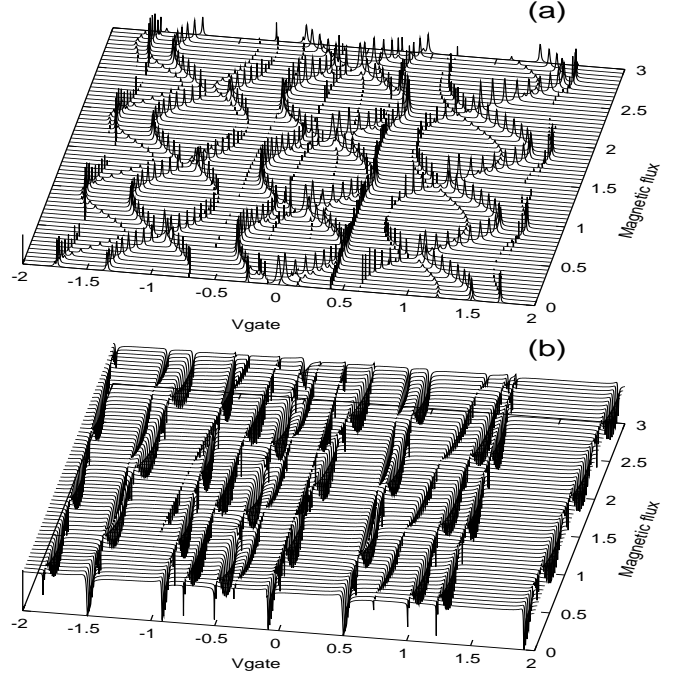


FIG. 2: The map of the nonflip-transmittance in the plane $(V_{gate}, \text{Magnetic flux})$ for two values of the Fermi energy: (a) $E_F = 0$ and (b) $E_F = 0.5$. The transition from the resonant to anti-resonant behavior can be noticed; the other parameters: $\tau = 0.2, J = -1$.

by the external leads). The multitude of parameters may give rise to different regimes and as an illustration we show in Fig.2 a map of the nonflip-conductance for two different values of E_F . One notices the change from a resonant behavior (panel a) to an anti-resonant one (panel b). At the same time, we have found that the flip-conductance keeps the resonant character for both values of the Fermi energy.

The understanding of the 3D picture in Fig.2 is relatively simple; one has to analyse separately the role played by the ring and by the dot in the transmittance process. Let us call $T_{\sigma\sigma'}^{(I)}$ the transmittance of the device in the case $\tau = 0$ (when the dot is completely detached from the ring) and express formally the transmittance as the sum of two contributions :

$$T_{\sigma\sigma'}(E, \Phi) = T_{\sigma\sigma'}^{(I)} + \tau^2 T_{\sigma\sigma'}^{(II)}, \quad (11)$$

where the second term is added when $\tau \neq 0$. Obviously, $T_{\sigma\sigma'}^{(I)}$ does not depend on the flux but may depend on the Fermi energy. Let us consider two situations :

a) the energy of the incident electron is such that $T_{\uparrow\uparrow}^{(I)} \approx 0$; then the second term describes the resonances of the ring-dot system, with a gate potential applied on the dot only.

b) the energy is such that $T_{\uparrow\uparrow}^{(I)} \lesssim 1$; since the total transmittance cannot be larger than 1, the only possible effect which can be produced by $T_{\uparrow\uparrow}^{(II)}$ is an antiresonance.

We succeeded to catch these two extreme cases in

Fig.2a and b, respectively, by choosing two different values of the Fermi energy. More complicated 3D patterns appear in intermediate situations. In what concerns the flip transmittance, obviously $T_{\uparrow\downarrow}^{(I)} = 0$ so that only the situation in panel (a) may occur and the flip transmittance will show always a resonant character.

III. SINGLET-TRIPLET REPRESENTATION FOR THE FLIP AND NON-FLIP PROPAGATORS.

In what follows we shall explain the Singlet-Triplet structure of the energy spectrum, the implication of the spectrum for the transport properties and the physical conditions ($T = 0$ and 'empty band' ground state [12]) under which one can get rigorous results.

For $S=1/2$ the natural formulation of the problem is in terms of singlet-triplet operators (see for instance [13]). One can define the fermion operators $\{d_{\uparrow}^{\dagger}, d_{\downarrow}^{\dagger}, d_{\uparrow}, d_{\downarrow}\}$ for the localized spin, provided one projects out all the states with occupancy different from 1, i.e. one has

$$n_d = d_{\uparrow}^{\dagger}d_{\uparrow} + d_{\downarrow}^{\dagger}d_{\downarrow} = 1. \quad (12)$$

Then, S_n^z , S_n^+ and S_n^- in eq (2) can be written as:

$$\begin{aligned} S_n^z &= \frac{1}{2}(d_{\uparrow}^{\dagger}d_{\uparrow} - d_{\downarrow}^{\dagger}d_{\downarrow}) \\ S_n^+ &= d_{\uparrow}^{\dagger}d_{\downarrow}, \quad S_n^- = d_{\downarrow}^{\dagger}d_{\uparrow}. \end{aligned} \quad (13)$$

Simultaneously we introduce the singlet operator Σ_i and the triplet operators T_i^p ($p=1,2,3$)

$$\begin{aligned} \Sigma_i &= \frac{1}{\sqrt{2}}(d_{\uparrow}c_{i\downarrow} - d_{\downarrow}c_{i\uparrow}) \\ T_i^1 &= \frac{1}{\sqrt{2}}(d_{\uparrow}c_{i\downarrow} + d_{\downarrow}c_{i\uparrow}) \\ T_i^2 &= d_{\uparrow}c_{i\uparrow} \\ T_i^3 &= d_{\downarrow}c_{i\downarrow}. \end{aligned} \quad (14)$$

The above operators may be used in order to write the Hamiltonian (2) in the following way (where we have used also $n_d = d_{\uparrow}^{\dagger}d_{\uparrow} + d_{\downarrow}^{\dagger}d_{\downarrow} = 1$):

$$\begin{aligned} H &= \sum_{\langle i,j \rangle} (w_{ij}^{\Sigma} \Sigma_i^{\dagger} \Sigma_j + w_{ij}^T \sum_p T_i^{p\dagger} T_j^p) \\ w_{ij}^{\Sigma} &= w_{ij} e^{i2\pi\Phi_{ij}} + \delta_{ij} Vg + \frac{3}{2} J \delta_{ij} \delta_{in} \\ w_{ij}^T &= w_{ij} e^{i2\pi\Phi_{ij}} + \delta_{ij} Vg - \frac{1}{2} J \delta_{ij} \delta_{in}. \end{aligned} \quad (15)$$

In the representation of $\{c, d\}$ -fermions, the propagation of the free electron corresponding to non-flip processes a) and b) and to the spin-flip process c) is described

by the following zero temperature two-time Green functions:

$$\begin{aligned} G_{ij}^a(E) &= \ll d_{\uparrow} c_{i\uparrow}; c_{j\uparrow}^{\dagger} d_{\uparrow}^{\dagger} \gg_E \\ G_{ij}^b(E) &= \ll d_{\downarrow} c_{i\uparrow}; c_{j\uparrow}^{\dagger} d_{\downarrow}^{\dagger} \gg_E \\ G_{ij}^c(E) &= \ll d_{\uparrow} c_{i\downarrow}; c_{j\uparrow}^{\dagger} d_{\downarrow}^{\dagger} \gg_E, \end{aligned} \quad (16)$$

where the ground state on which the Green functions are defined should be explained. From now on the state $|>_0$, on which the Green functions are defined, will be chosen as the vacuum with respect to both c - and d -fermions. This is the so-called 'empty band' approach for the electronic problem. With this choice the propagators (16) describe the propagation of a "test" electron through the interferometer containing the localized spin. The same single electron approach is considered by Menezes et al [15] and Joshi et al [16] when using the wave guide approach for the ring+flipper problem in the continuum representation (they do not emphasise the natural singlet-triplet formulation of the problem). Using the same approach Nolting obtained rigorous results for the the electron excitation spectrum of ferromagnetic semiconductors [12].

The generic equation of motion satisfied by these functions is (see the discussion in Appendix):

$$E \ll A; B \gg_E = \ll [A, B]_+ \gg_0 + \ll [A, H^{eff}]_- \gg_E. \quad (17)$$

As an example, the equation of motion for G^c reads:

$$\begin{aligned} (E - V_g) G_{ij}^c &= \sum_k w_{ik}(\Phi) G_{kj}^c + \tau_0^2 e^{-iq} \sum_{\alpha} \delta_{i\alpha} G_{\alpha j}^c \\ &+ \delta_{in} \frac{J}{2} G_{ij}^c - \delta_{in} J G_{ij}^b - \delta_{in} \frac{J}{2} \ll d_{\downarrow}^{\dagger} d_{\downarrow} d_{\uparrow} c_{i\downarrow}; c_{j\uparrow}^{\dagger} d_{\downarrow}^{\dagger} \gg \\ &+ J \ll c_{n\downarrow}^{\dagger} c_{n\uparrow} c_{i\downarrow} d_{\downarrow}; c_{j\uparrow}^{\dagger} d_{\downarrow}^{\dagger} \gg + J \ll d_{\uparrow}^{\dagger} d_{\uparrow} d_{\downarrow} c_{i\uparrow}; c_{j\uparrow}^{\dagger} d_{\downarrow}^{\dagger} \gg \\ &- \frac{J}{2} \ll d_{\uparrow}^{\dagger} (c_{n\uparrow}^{\dagger} c_{n\uparrow} - c_{n\downarrow}^{\dagger} c_{n\downarrow}) c_{i\downarrow}; c_{j\uparrow}^{\dagger} d_{\downarrow}^{\dagger} \gg \end{aligned} \quad (18)$$

With our choice for the ground state, exact results are obtained as the equation of motion get closed without any approximation. Indeed, now all "higher" Green functions

$$\begin{aligned} &\ll d_{\uparrow}^{\dagger} (c_{n\uparrow}^{\dagger} c_{n\uparrow} - c_{n\downarrow}^{\dagger} c_{n\downarrow}) c_{i\downarrow}; c_{j\uparrow}^{\dagger} d_{\downarrow}^{\dagger} \gg, \\ &\ll c_{n\downarrow}^{\dagger} c_{n\uparrow} c_{i\downarrow} d_{\downarrow}; c_{j\uparrow}^{\dagger} d_{\downarrow}^{\dagger} \gg, \end{aligned} \quad (19)$$

etc, vanish.

We remind that if the Fermi sea is considered as the ground state, the "higher" Green functions do not vanish any more and the solution can be found only approximately, using specific decoupling procedures (see, for instance [13, 14]).

Eq.(18) becomes :

$$\begin{aligned} \sum_k [(E - V_g - \tau_0^2 e^{-iq} \sum_{\alpha} \delta_{i\alpha} - \frac{J}{2} \delta_{in}) \delta_{ik} - w_{ik}] G_{kj}^c(E) \\ = -\delta_{in} J G_{ij}^b(E). \end{aligned} \quad (20)$$

One can verify that $\langle \Sigma_i H T_j^{p\dagger} \rangle_0 = 0$, meaning that the Hilbert space $\mathcal{H}_{2N}^\sigma \otimes \mathcal{H}_2^S$ splits as follows:

$$\mathcal{H}_{2N}^\sigma \otimes \mathcal{H}_2^S = \mathcal{H}_N^\Sigma \oplus \mathcal{H}_{3N}^T.$$

The singlet and triplet-type eigenenergies can be obtained by the diagonalization of the matrices w_{ij}^Σ and w_{ij}^T , respectively.

It is useful to define the singlet and triplet propagators

$$G_{ij}^\Sigma(E) = \langle\langle \Sigma_i; \Sigma_j^\dagger \rangle\rangle_E, \quad G_{ij}^{T(p)}(E) = \langle\langle T_i^{(p)}; T_j^{(p)\dagger} \rangle\rangle_E$$

as these functions satisfy decoupled equations of motion:

$$\sum_{k=1}^N [(E\delta_{ik} - w_{ik}^\Sigma - \tau_0^2 e^{-iq} \sum_{\alpha} \delta_{i\alpha} \delta_{\alpha k}) G_{kj}^\Sigma(E) = \delta_{ij}, \quad (21)$$

$$\sum_{k=1}^N [E\delta_{ik} - w_{ik}^T - \tau_0^2 e^{-iq} \sum_{\alpha} \delta_{i\alpha} \delta_{\alpha k}] G_{kj}^{T(p)}(E) = \delta_{ij}, \quad (22)$$

where w^Σ and w^T are defined in eq(17). The Green functions for the three triplet states are identical, so we shall skip the upper index of T . When obtaining equations (21) and (22) the symmetry relations

$$\begin{aligned} \langle\langle d_{\downarrow} c_{i\uparrow}; c_{j\downarrow}^\dagger d_{\uparrow}^\dagger \rangle\rangle &= \langle\langle d_{\uparrow} c_{i\downarrow}; c_{j\uparrow}^\dagger d_{\downarrow}^\dagger \rangle\rangle \\ \langle\langle d_{\downarrow} c_{i\uparrow}; c_{j\uparrow}^\dagger d_{\downarrow}^\dagger \rangle\rangle &= \langle\langle d_{\uparrow} c_{i\downarrow}; c_{j\downarrow}^\dagger d_{\uparrow}^\dagger \rangle\rangle \end{aligned}$$

have been used.

It turns out from their definitions that the three propagators describing the processes a), b) and c) can be expressed in terms of singlet and triplet propagators as follows

$$\begin{aligned} G^a &= G^T \\ G^b &= (G^T + G^\Sigma)/2 \\ G^c &= (G^T - G^\Sigma)/2 \end{aligned} \quad (23)$$

The above relations show that the non-flip process a) is purely triplet-type since only the matrix w^T enters the dynamics of the propagator G^a , while the non-flip process b) and the flip process c) involve both the triplet and singlet states. We note that from (22) we recover the expression of G^T given by (10) in the previous section.

IV. THE SIMPLEST SPIN INTERFEROMETER

By the use of eq.(21-22) and (23) it is now very easy to analyse analytically the simple example of a triangular spin interferometer placed in magnetic field. In this way we get hints for understanding the complex system.

We present first the energy spectrum (with Singlet-Triplet structure) versus the enclosed flux (Fig.3). The distance between a Singlet-Triplet pair of levels is, of course, controlled by the exchange parameter, but there

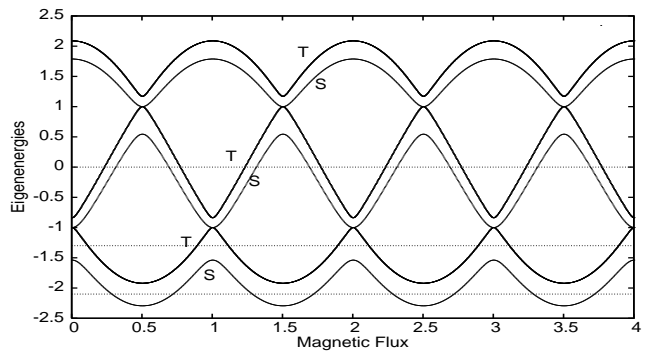


FIG. 3: The energy spectrum of the simplest (triangular) spin interferometer as function of the magnetic flux. The singlet (S) and the triplet (T) eigenvalues are indicated. The three horizontal lines represent possible positions of E_f ; exchange parameter $J = -0.5$.

are also degeneracy points which are independent of J as we shall explain below.

In order to study the transport, we connect ideal leads to the sites we shall refer to as "1" and "3" using the hopping constant τ_0 . The flipper is located on the site "2". The sites of the triangle are interconnected by the hopping parameter $e^{\pm i2\pi\Phi/3}$ (the total encircled flux Φ is measured in quantum flux units). We find the solution of eq.(21-22) as :

$$G_{13}^{\Sigma,T}(E) = e^{i2\pi\Phi/3} \frac{e^{-i2\pi\Phi} + (E - \alpha^{\Sigma,T})}{\Delta}, \quad (24)$$

$$\begin{aligned} \Delta &= (E - \tau_0^2 e^{-iq})^2 (E - \alpha^{\Sigma,T}) - 2(E - \tau_0^2 e^{-iq}) \\ &\quad - (E - \alpha^{\Sigma,T}) - 2\cos(2\pi\Phi), \end{aligned} \quad (25)$$

with $\alpha^\Sigma = J\frac{3}{2}$ and $\alpha^T = -J\frac{1}{2}$. One can notice that, while the module of $G^{\Sigma,T}(E)$ is symmetrical under flux reversal and has the $\Phi_0 = 1$ flux periodicity, its phase is *not* symmetrical under flux reversal and has a $3\Phi_0$ periodicity due to the factor $e^{i2\pi\Phi/3}$. On the other hand, the phase difference between G^T and G^Σ (i.e., $\Delta\lambda_{T\Sigma} = \text{atan}(\text{Im}G^T/\text{Re}G^T) - \text{atan}(\text{Im}G^\Sigma/\text{Re}G^\Sigma)$), which is important for the processes b) and c) (as expressed by eq.23), is periodic with Φ_0 but remains asymmetric under flux reversal. This explains why the transmittances assigned to the processes b) and c) are asymmetric under flux reversal, as also found by Joshi et al[16].

For $\tau_0 = 0$ the zeros of Δ in Eq.27 give the energy spectrum. For integer (semi-integer) values of the flux the energy $E = -1$ ($E = 1$) is an eigenvalue independent of $\alpha^{\Sigma,T}$ meaning that the triplet and the singlet are degenerated as it can be seen in Fig.3.

Looking at the spectrum, we can realize that G^Σ and G^T (that is also the propagator for the a) process) will show, each of them, one or two peaks per period, depending on the E_f (see the horizontal lines in the spectrum

figure). As a result, G^c and G^b may show up to four peaks per period in the case of the weak coupling with the leads. However, for strong coupling, neighbouring singlet and triplet peaks will overlap with either constructive or destructive effect, depending on the phase difference $\Delta\lambda_{T\Sigma}$ (see Fig.4c).

As the magnetic flux is changed, the T and S levels cross the Fermi energy giving rise to the addition or loss of one electron at each cross. Taking into account that the addition of an electron corresponds to a phase increase of π (and vice versa) the evolution of $\Delta\lambda_{T\Sigma}$ in Fig.4a is easily understood, when the peaks are well separated in the case of weak coupling. As we increase the coupling, the peaks are broadening and we can see in Fig.4c that the first pair of peaks evolves into a single big peak while the second pair vanishes corresponding to a phase difference $\Delta\lambda_{T\Sigma} \approx 0$.

V. THE SPECTRUM AND SPIN TRANSMITTANCE OF THE RING+2D DOT INTERFEROMETER

In the following we shall continue the numerical analysis of the real system consisting of the ring+2D quantum dot (with magnetic impurity). In order to show the complexity of the problem, we present first a detail of the energy spectrum of our system (Fig.5). In Fig.5a the dot is decoupled from the ring; the levels of the 2D finite dot (shown in solid line) depend on the magnetic field and can be indexed as Triplet and Singlet levels, while the levels of the truncated ring (dotted line) are invariant with Φ . Obviously, when we increase the ring-dot coupling τ the levels undergo hybridization. As long as the ring-dot hybridization is weak (as in Fig.5b) and we are sufficiently far away from the self-avoiding points, the eigenvalues can still be identified as ring-like or dot-like. The ring-like levels begin to oscillate with the (approximate) Φ_0 period and each one splits also into a Singlet and a Triplet; obviously the splitting depends on the value of the exchange J , and on the hybridization determined by the ring-dot coupling τ and on the relative distance between levels.

For strong hybridization (see Fig.5c) the dot-like levels begin also to exhibit Φ_0 oscillations superimposed over their usual slow dependence on the flux observed in Fig.5a. One can notice that the dot-like levels are intercalated between singlet-triplet pairs of ring-like levels; this occurs because the exchange splitting of the dot-like levels is much bigger than the splitting of the ring-like levels. In fact, for strong ring-dot coupling, the spectrum becomes complicated and it is difficult to identify any more the origin of different eigenvalues.

Now we continue the numerical analysis of the spin transmittance in the limit of perfect ring-leads coupling ($\tau_0 = 1$), which meets the usual experimental conditions

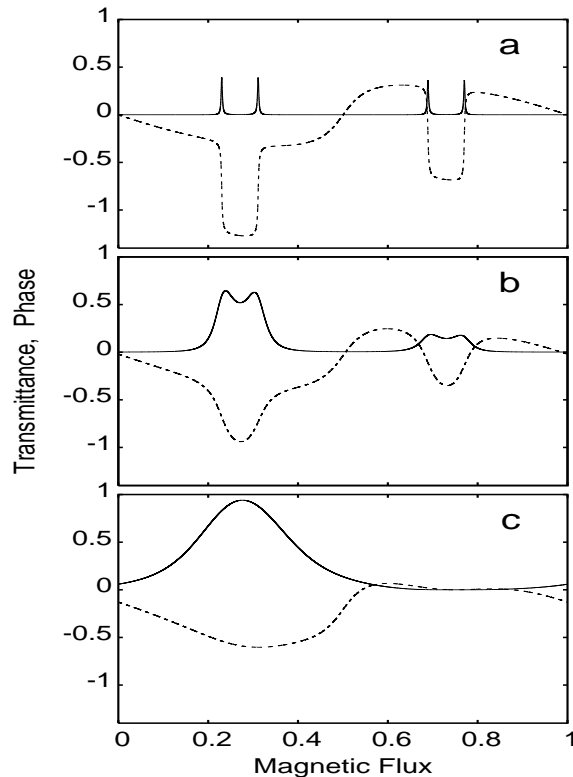


FIG. 4: Flip transmittance (solid line) for the triangular spin interferometer, plotted together with the phase difference $\Delta\lambda_{T\Sigma}$ (dashed line, in π units) for three couplings with the leads : a) $\tau_0 = 0.2$, b) $\tau_0 = 0.4$, c) $\tau_0 = 1.0$; the other parameters are $J = -0.5$, $E_f = 0$.

for studying the AB oscillations.

Since the spin-up and the spin-down waves cannot interfere, being orthogonal and corresponding to two different channels, the flip-interference process can only take place between the flipped electron wave transmitted through the dot and the flipped wave reflected by the dot; this introduces a difference in phase compared to the nonflip process and explains why the flip-interference may be destructive at values of the magnetic field where the direct (nonflip) process is constructive. Another effect is the accumulation of phase in the dot which will affect the Fourier spectra of the spin-dependent magnetoconductance fluctuations.

The interference pattern as function of the magnetic flux through the ring depends specifically on the characteristics of the quantum dot, namely, by its coupling to the ring and the properties of the energy spectrum described above. Implicitly, the position of the Fermi level becomes important.

For weak ring-dot coupling, the AB oscillations come from the participation in transport of the ring-like levels that have a (approximate) Φ_0 periodicity and show a Singlet-Triplet splitting (the case shown in Fig.5b). This splitting is however very small since the localized mag-

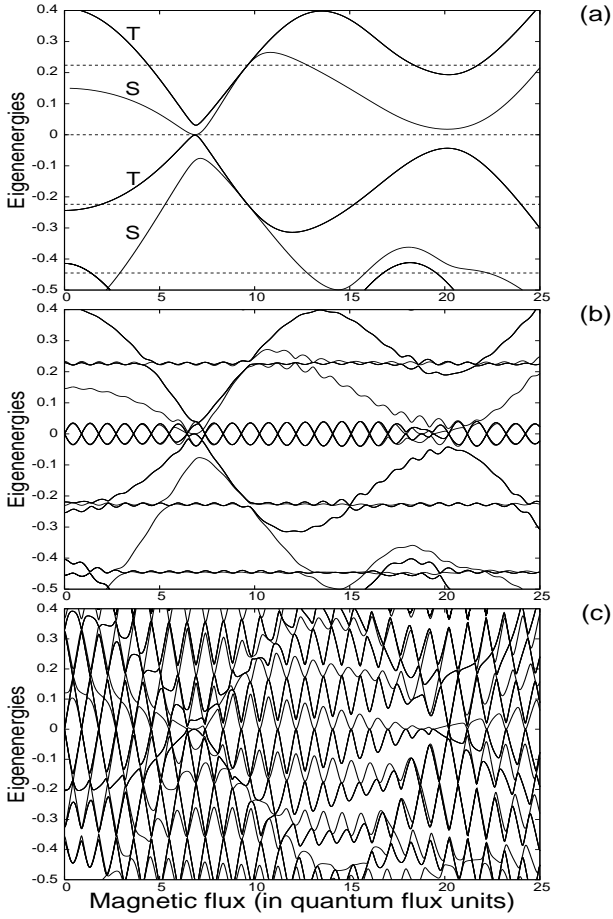


FIG. 5: Spectrum of the ring-dot (with magnetic impurity) system for the cases: a) The dot is decoupled from the ring ($\tau = 0$). The levels of the 2D dot (solid line) show flux dependence and strong Singlet(S)-Triplet(T) splitting ; the levels of the truncated ring (dotted line) are constant. b) Moderate ring-dot coupling ($\tau = 0.4$) . Both dot and ring levels undergo hybridization. The levels of the ring have a (approximate) Φ_0 oscillation period and a very small S-T splitting that becomes more visible in the case c) Strong ring-dot coupling ($\tau = 1.0$) with strong hybridization of levels.

netic impurity is placed in the dot and acts like a small perturbation for the "ring" levels. Then, one can assume that $|G^T| \approx |G^\Sigma|$ and the phase difference $\lambda_{T,\Sigma} \approx 0$, except for those intervals of flux where the dot levels get involved in transport. As a result the flip oscillations, being proportional to $|G^T - G^\Sigma|$, are much smaller than the nonflip oscillations given by G^a or G^b .

The position of the Fermi energy is very important for the general aspect of the oscillation pattern. When the Fermi energy crosses (or is close to) the oscillating ring-like levels, both the nonflip and flip transmittances show regular oscillations (much reduced for the flip case), with anomalies in those domains of the flux where dot-like levels are also involved in transport .

Even if the Fermi energy is far from the ring levels the

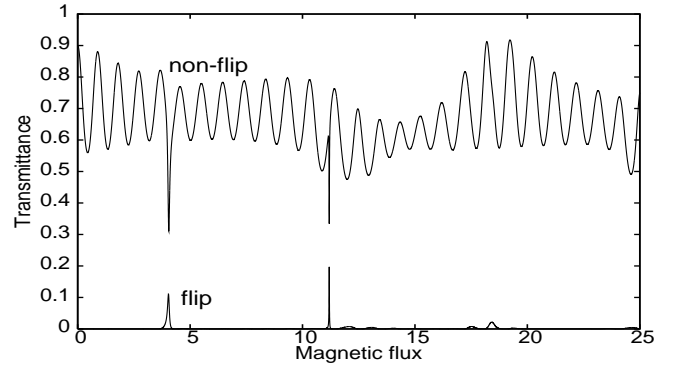


FIG. 6: The two components -nonflip and flip- of the transmittance as function of the magnetic flux Φ through the ring (parameters: $\tau = 0.4$, $J = -1$, $V_{gate} = 0$, $E_F = -0.35$). The non-flip transmittance exhibits usual oscillations, while the flip has peaks when the dot levels cross the Fermi energy.

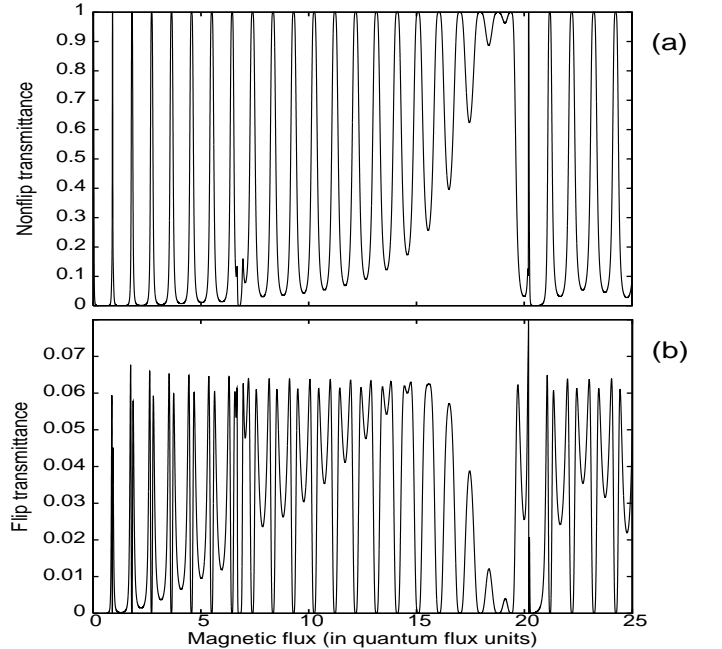


FIG. 7: The two components of the transmittance as function of the magnetic flux Φ through the ring: (a) nonflip $T_{\uparrow\uparrow}$, (b) flip $T_{\uparrow\downarrow}$ (parameters: $\tau = 1$, $J = -1$, $V_{gate} = 0$, $E_F = 0$). Note the double peak structure of the flip and the complementary windows in the range $[15-20\Phi_0]$.

nonflip transmittance behaves similarly. On the contrary, the flip transmittance does not show oscillations but has only peaks at values of the flux where the dot levels cross E_F . In this way the energy levels of the dot can be identified by the flip transmittance. We illustrate this situation in Fig.6.

For the strong ring-dot coupling $\tau = 1$, the spectrum shown in Fig.5c plays the game and the result consists in

strong oscillations for any Fermi level. Four peaks per period cannot be observed since the splitting is small compared to the broadening induced by the strong coupling of the system to the leads $\tau_0 = 1$. The general picture is that one of single or double peak per period both for the flip and non-flip transmittance, depending however on the E_F . The double peak is usually asymmetric as in Fig.4b of the triangle model.

A peculiar situation, when the spin effect is strong, occurs at $E_F = 0$ and is shown in Fig.7. The difference noticed between the panels (I) and (II) is due to the fact that the scattering processes (b=nonflip) and (c=flip) combine in different ways the singlet and triplet propagators. The situation is presented at a better resolution in Fig.8a, and it can be noticed that T_{\downarrow} is nearly zero in the same place where $T_{\uparrow} \approx 1$. With necessity, the quasi-zero of the flip transmittance occurs when $|G^T| \approx |G^\Sigma|$ and $\lambda_{T,\Sigma} \approx 0$. Under the same circumstances, the non-flip process (b) described by $|G^T + G^\Sigma|$ has a maximum value. This explains the destructive interference of the flip process at the same value of the flux where non-flip interference process is constructive. It can also be noticed that the transmittance varies strongly in some domains (as for instance between $15 - 20\Phi_0$). A separate calculation indicates that the transmission of the dot is much suppressed in these domains, while the amplitude of T_{\uparrow} through the lower arm is close to 1; these two facts yield the picture shown in Fig.7a. On the other hand, when the transmission through the dot is low, the probability of the flip process is reduced explaining the complementary window of the T_{\downarrow} in Fig.7b.

We have checked that such windows are a combined effect of the presence of the dot and of the magnetic impurity; it turns out, however that for $E_F = 0$ the windows in the interference pattern comes from the exchange.

One can observe in the top panel of the Fig.8 that the large peak representing the nonflip-interference embraces the double peak representing the flip-process. The splitting increases with the exchange J and hence the width of the large peak depends also on this parameter.

An important instrument for the analysis of the transmittance oscillations is the Fourier transform [10]. The Fourier spectra of T_{\uparrow} and T_{\downarrow} are shown in Fig.8b and Fig.8c in the case of the perfect coupling between the dot and the ring ($\tau = 1$). The fact that already the first interference process occurs with the participation of a reflected wave results in the reduction of the first maximum in the Fourier spectrum for the flip-channel.

The coupling τ is important for the aspect of the Fourier spectrum because any constriction at the dot gives rise to a reflection of the spin-up electron, and changes the aspect of the Fourier spectrum of T_{\uparrow} , that might become similar to the spectrum of T_{\downarrow} .

When the dot is attached to the ring the positions of the interference peaks are shifted due to an accumulation of phase in the dot; this effect is clearly visible in

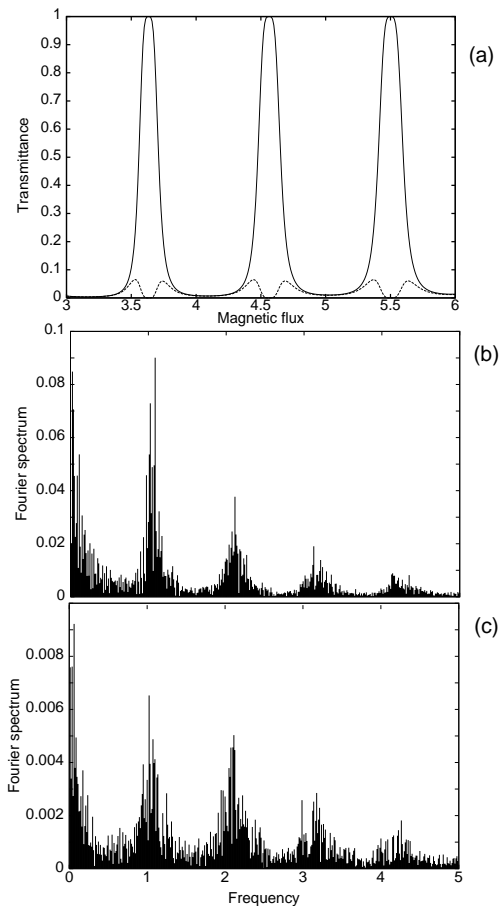


FIG. 8: (a) The double-peak structure of T_{\downarrow} embraced by the large peak of T_{\uparrow} . The Fourier spectrum corresponding to the curves shown in FIG.3: (b) the nonflip component. (c) the flip component shows more noise and a reduced value of the first maximum as the result of the specific interference process (parameters: $\tau = 1, J = -1, V_{gate} = 0, E_F = 0$).

the Fourier spectrum of the AB oscillations, namely the positions of the maxima do not coincide any more with the integer multiples of the $2\pi/\Phi_0$, which are characteristic to the individual ring. The shift can be noticed both in Fig.8b and Fig.8c for the non-flip and flip transmittance, respectively. In the mesoscopic physics, the Fano effect is the consequence of the hybridization between the continuum spectrum of the leads and the discrete spectrum of the meso-system [11]. The asymmetric shape of the transmittance peaks, the occurrence of zeros, and the behavior of the transmittance phase on the resonances and between them are the aspects of interest.

In the system under consideration, the dependence on the gate potential (at fixed magnetic field) of the transmittance phases corresponding to different flip and non-flip processes show the usual behavior and we shall not insist on these aspects: the phase increases with π on each resonance and there are also discontinuous jumps with $\pm\pi$ between the resonances with the same parity,

where the transmittance vanishes [8]. Since in our case the magnetic field is non-zero, these jumps do not represent true Fano zeros because the real and imaginary part of the transmittance amplitude cannot change simultaneously the sign. Nevertheless, when the change in sign of ReT and ImT occurs at close values of the gate bias, the variation of the phase is still abrupt. Then, the jump of the phase can be upwards (with a gain of π) or downwards (with a loss of π); obviously, the difference is given by the sign of ImT at $ReT = 0$ (which is positive in the first case and negative in the second one).

On the other hand, the phase have a very complex behavior as function of magnetic field. Some analysis can be made for the simple triangle model, where we can study separately the phase of the denominator and of the numerator in Eq.(24). The two contributions are easy to be identified for $\tau_0 \ll 1$ when the resonances are narrow. Then the phase of the denominator Δ (eq(25)) has a sudden evolution with π and $-\pi$ on consecutive resonances, but remains constant in between. On the other hand, the phase of the numerator, which in fact does not depend on τ_0 , has a very small evolution on the narrow resonances and is responsible for the monotonic increase (or decrease, depending on E_F) of the phase of $G_{13}^{\Sigma,T}$ between resonances. We note that the numerator of these propagators vanishes only incidentally for $E - \alpha^{\Sigma,T} = \mp 1$ and integer (semi-integer) values of the flux, In the limit $\tau_0 \rightarrow 1$ the width of the resonances increases causing the overlap of neighbouring resonances and a 'bump' instead of a $\mp\pi$ evolution of the phase at the variation of the flux.

The non-monotonic variation of the phase on the peak indicates that the phasor of the transmittance in the complex plane (ReT, ImT) has a turning point (as shown in Fig.9b and Fig.9d).

When extending this analysis to the complex system we realize that the numerator becomes a very complicated trigonometric function and exact zeros, and even quasi-zeros, may exist only incidentally. So, the general aspect of the phase consists in a smooth dependence on flux between two consecutive peaks and a bump on each peak.

The special situation when the phase indicates quasi Fano zeros has been found numerically at $E_F = 0$ for the case of impurity free dot ($J = 0$); however, the usual behavior is recovered in the presence of the exchange ($J \neq 0$). The two situations are shown in Fig.9. In the same figure we give also the phase of the process (c), which is obtained by combining the phases and modules of the G^T and G^Σ for the complex ring-dot system.

VI. CONCLUSIONS

In conclusion, in this paper we report the first calculation of the spin-dependent transmittance through an

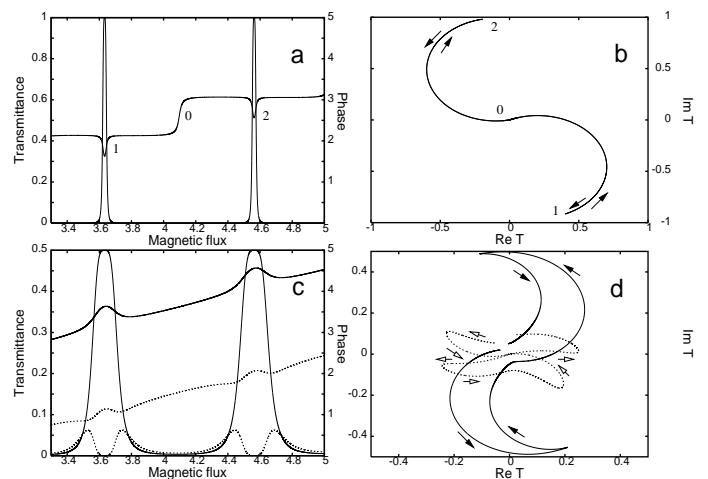


FIG. 9: a) Transmittance and phase for the impurity-free system ($J=0$); b) The corresponding evolution of the phasor (ImT vs ReT). The points 1,0,2 correspond to the same points in the panel (a). The arrows indicate the evolution of the phasor with increasing flux in the range $[3.3 - 5.0\Phi_0]$. c) Transmittance and phase for the Triplet (solid line) and the Flip (dashed line); d) The corresponding evolution of the phasors. The phasor of the Flip (amplified for better visibility) has four turning points corresponding to the four peaks of the flip-transmittance in panel (c).

interferometer consisting of a ring with embedded two-dimensional dot doped with magnetic impurities. For the time being, there are no experiments to be compared with, but they are expected in the near future, and our goal is to make predictions. The study is based on the spectral analysis and a suitable transport formalism which has been developed for the single-particle case.

The aspect of the Aharonov-Bohm oscillations depends strongly on the Fermi energy and the ring-dot and ring-leads coupling parameters. Generally, the oscillations exhibit single or double asymmetric peaks per period as it is suggested by the analytically solvable triangular model. The flip oscillations are much reduced in amplitude compared to the nonflip ones. The finite size of the dot, combined with the effect of the impurity, gives rise to windows in the interference pattern where the flip and nonflip components of the transmittance behave in a complementary way. In the case of weak ring-dot coupling the AB oscillations of the flip channel may cease to exist, the flip magnetoconductance showing instead peaks corresponding to the levels of the dot. The general aspect of the transmittance phase of the AB oscillations consists in bumps on the oscillation peaks and a monotonic behavior between them.

In order to explain these properties we have expressed the different physical tunneling processes in terms of singlet and triplet propagators, which is the natural formulation of the problem.

Acknowledgments The support of DFG /SFB 608

and the Romanian CERES Programme is acknowledged. We thank M.Nita and V.Dinu for very useful discussions.

APPENDIX

We introduce the Hamiltonian of the semi-infinite non-interacting leads H^L and the lead-ring coupling H^{LR} . The different leads are indexed by α , which stands also for the site where the lead is attached. Then,

$$H^L = \sum_{\alpha\sigma} \sum_{n=0}^{\infty} c_{n\sigma}^{\alpha\dagger} c_{n+1\sigma}^{\alpha} + H.c. \quad (26)$$

$$H^{LR} = \tau_0 \sum_{\alpha\sigma} c_{0\sigma}^{\alpha\dagger} c_{\alpha\sigma} + H.c., \quad (27)$$

where τ_0 is the hopping integral between the first site on the lead, $n = 0$, and the site α on the ring.

The Hamiltonian of the whole system is

$$H^{total} = H + H^L + H^{LR}, \quad (28)$$

where H was defined already in (2). Let us introduce also

$$H^{eff} = H + \tau_0^2 e^{-iq} \sum_{\alpha\sigma} c_{\alpha\sigma}^{\dagger} c_{\alpha\sigma}, \quad (29)$$

where $E = 2\cos(q)$ is the energy of the incident 'test' electron. We have to prove that

$$\ll [d_{\uparrow}c_{i\downarrow}, H^{Total}]; c_{j\uparrow}^{\dagger}d_{j\downarrow}^{\dagger} \gg = \ll [d_{\uparrow}c_{i\downarrow}, H^{eff}]; c_{j\uparrow}^{\dagger}d_{j\downarrow}^{\dagger} \gg,$$

meaning that the effective Hamiltonian H^{eff} can be used instead of H^{total} . This will be valid if the Green functions are defined on the vacuum at zero temperature. The proof is given for G^c but the same is true for all the functions in (16).

Performing the commutators, one gets (we write only the non-vanishing terms):

$$\ll [d_{\uparrow}c_{i\downarrow}, H^L + H^{LR}]; c_{j\uparrow}^{\dagger}d_{j\downarrow}^{\dagger} \gg = \delta_{i\alpha}\tau_0 \ll d_{\uparrow}c_{0\downarrow}^{\alpha}; c_{j\uparrow}^{\dagger}d_{j\downarrow}^{\dagger} \gg$$

and,

$$\begin{aligned} \ll [d_{\uparrow}c_{i\downarrow}, \tau_0^2 e^{-iq} \sum_{\alpha\sigma} c_{\alpha\sigma}^{\dagger} c_{\alpha\sigma}]; c_{j\uparrow}^{\dagger}d_{j\downarrow}^{\dagger} \gg = \\ \delta_{i\alpha}\tau_0^2 e^{-iq} \ll d_{\uparrow}c_{\alpha\downarrow}; c_{j\uparrow}^{\dagger}d_{j\downarrow}^{\dagger} \gg. \end{aligned}$$

In order to show that these two expressions are equal, we define

$$g_n =: \ll d_{\uparrow}c_{n\downarrow}^{\alpha}; c_{j\uparrow}^{\dagger}d_{j\downarrow}^{\dagger} \gg,$$

which satisfy the following equations of motion:

$$\begin{aligned} E g_0 &= g_1 + \tau_0 \ll d_{\uparrow}c_{\alpha\downarrow}; c_{j\uparrow}^{\dagger}d_{j\downarrow}^{\dagger} \gg, \\ E g_n &= g_{n-1} + g_{n+1}, \quad n = 1, 2, \dots \end{aligned} \quad (30)$$

The solution of eqs (30) is

$$g_n = \tau_0 e^{-iq(n+1)} \ll d_{\uparrow}c_{\alpha\downarrow}; c_{j\uparrow}^{\dagger}d_{j\downarrow}^{\dagger} \gg. \quad (31)$$

so that, finally,

$$\ll d_{\uparrow}c_{0\downarrow}^{\alpha}; c_{j\uparrow}^{\dagger}d_{j\downarrow}^{\dagger} \gg = \tau_0 e^{-iq} \ll d_{\uparrow}c_{\alpha\downarrow}; c_{j\uparrow}^{\dagger}d_{j\downarrow}^{\dagger} \gg, \quad (32)$$

which concludes the demonstration that in this case the use of H^{eff} is equivalent to the use of H^{total} .

-
- [1] A.Yacoby, M. Heiblum, D.Mahalu and H.Shtrikman, Phys.Rev.Lett.**74**, 4047 (1995); R.Schuster, E.Bucks, M. Heiblum, D.Mahalu, V.Umanski and H.Shtrikman, Nature **385**,417, (1997); Y.Ji, M.Heiblum, and H.Shtrikman, Phys.Rev.Lett.**88**,076601 (2002); K.Kobayashi, H.Aikawa, S.Katsumoto, and Y.Iye, Phys.Rev.Lett.**88**,256806 (2002).
 - [2] G.Hackenbroich and H.A. Weidenmüller, Phys.Rev.B, **53**,16379 (1996); A.Aharony, O.Entin-Wohlman, Y. Imry, Phys.Rev.Lett.**90**,156802 (2003).
 - [3] O.Sakai, W.Izumida, preprint cond-mat 0208505; K.Kang, L.Craco, Phys.Rev.B **65**, 033302 (2001); H.Hu, G-M.Zhang and L.Yu, Phys.Rev.Lett **86**,5558 (2001).
 - [4] T.Nakanishi, K.Terakura and T.Ando, Phys.Rev.B, **69**, 115307 (2004).
 - [5] H.Aikawa, K.Kobayashi, A.Sano, S.Katsumoto and Y. Iye, Phys.Rev.Lett. **92**, 176802 (2004).
 - [6] for a ring of radius $50nm$, described in the TB model by 32 sites on the ring, and for J of the order of the hopping integral ($w \approx 5meV$) this condition is fulfilled at $B < 200T$ (the g-factor of GaAs has been considered).
 - [7] A.Aldea, P.Gartner and I.Corcotoi, Phys.Rev.B **45**, 14122 (1992); J.Wu, B.L.Gu, H.Chen, W.Duan, Y.Kawazoe, Phys.Rev.Lett. **80**,1952 (1998).
 - [8] A.L. Yeyati and M.Büttiker, Phys.Rev.B **62**, 7307 (2000);
 - [9] V.Moldoveanu, A.Aldea, A.Manolescu, and M.Niță, Phys. Rev B, **63**, 045301 (2001); V. Moldoveanu, A. Aldea and B. Tanatar, Phys. Rev. B **70**, 085303 (2004).
 - [10] S.Washburn and R.A.Webb, Advances in Physics,**35**, 375 (1986).
 - [11] H.Xu and W.Sheng, Phys.Rev.B **57**, 11903 (1998); O. Entin-Wohlman, A.Aharony, Y.Imri and Y. Levinson, cond-mat 0109328;
 - [12] W.Nolting, J.Phys.C:Solid State Phys. **12**,3033 (1979); W.Nolting, *Grundkurs:Theoretische Physik,7.Viel-Teilchen-Theorie*, ch.4.5.4, p.293, Verlag Zimmermann-Neufang, 1992.
 - [13] G.Horwitz, S.Alexander, and M.Fibich, Phys.Rev.**168**, 495 (1968).
 - [14] Y.Nagaoka Phys.Rev.**138**, A1112 (1965).
 - [15] O.L.T. de Menezes and J.S.Helman, Am. J. Phys. **53**, 1100 (1985)
 - [16] S.K. Joshi, D. Sahoo, and A.M. Jayannavar, Phys.Rev.B, **64**, 075320 (2001).